Optic Disc and Optic Cup Segmentation on Retinal Image Based on Multimap Localization and U-Net Convolutional Neural Network

A. N. Almustofa, A. Handayani, and T. L. R. Mengko
Department of Biomedical Engineering, School of Electrical Engineering and Informatics, Bandung Institute of Technology, Bandung, Indonesia
Email: anasnafis77@gmail.com, a.handayani@ieee.org, tmengko@itb.ac.id

***Abstract*—Glaucoma is an eye disease that is caused by an increase in intraocular pressure. Excessive intraocular pressure could damage optic nerves and lead to vision loss. Early detection is crucial to treat the patient as fast as possible to prevent irreversible blindness. Glaucoma diagnosis can be supported by a computer-aided detection system that provides automated measurement of the physical dimensions of the optic disc and the optic cup from retinal images. The Cup to Disc Ratio (CDR) of these measurements indicates the risk of developing glaucoma. CDR calculation relies on accurate optic disc localization and optic disc/cup segmentation. In this research, we developed an unsupervised optic disc localization and optic disc/cup semantic segmentation using U-Net which is optimized for retinal images from the Drishti-GS and Refuge datasets. 99.99±0.12% of the optic disc pixels were correctly included in the regions of interest by the proposed localization method. Further semantic segmentation on the regions of interest yields F-scores of 0.935±0.031 (Drishti-GS) and 0.950 ± 0.028 (Refuge) for optic disc and 0.832±0.071 (Drishti-GS) and 0.871±0.061 (Refuge) for optic cup. These results are comparable to the state-of-the-art methods.**

***Index Terms*—glaucoma, optic disc, optic cup, localization, segmentation**

I. INTRODUCTION

Glaucoma is an eye disease that is caused by an increase of intraocular pressure due to blockage of aqueous humor drainage. Excessive intraocular pressure induces damages to the optical nerves which may lead to the loss of eyesight. Hence, early treatment is crucial to prevent the patient from irreversible blindness. Unfortunately, most patients are often unaware if they had developed early-stage glaucoma. Based on data from the Health Ministry of Indonesia [1], about 51.4% of open-angle and 41.4% of closed-angle glaucoma cases were detected in the advanced stages. Furthermore, about 13.5% and 26.4% of patients with open-angle and closed-angle glaucoma respectively develop irreversible blindness. Hence, routine eye checkups of the potential patients will help to detect the early development of glaucoma.

Manuscript received December 17, 2021; revised June 20, 2022.

Besides visual field test, there are two other methods to diagnose glaucoma. The first method is by measuring the Intraocular Pressure (IOP) using a tonometer. High pressure on the tonometer indicates the presence of glaucoma. However, this method is uncomfortable for the patient due to the invasiveness of the tonometer. The second method is through an ophthalmoscopic observation of the dimensional change in the Optical Nerve Head (ONH). This method is preferable to the first one as it is less invasive. The optic cup of the ONH tends to be larger in glaucoma patients due to thinning of the cup region. Fig. 1 depicted the ONH appearance in glaucoma and non-glaucoma cases.

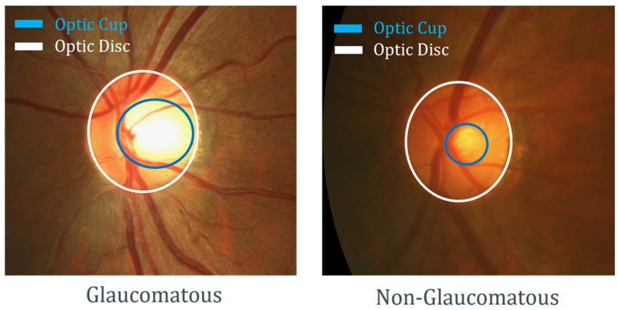

Figure 1. Optical Nerve Head (ONH) appearance in glaucomatous and non-glaucomatous cases.

Enlargement of the optic cup can be identified by measuring several features such as Cup-to-Disc Ratio (CDR), optic disc diameter, Peripapillary Atrophy (PPA), and neuroretinal rim [2]. Despite different opinions about the effectiveness of these features in glaucoma assessment, CDR is the feature that is most acceptable and used in the previous study [3]. CDR is calculated from the ratio of the optic cup and disc spatial features such as diameter or area. In glaucomatous case, CDR tends to be higher than certain threshold value (around 0.4–0.6).

Previously, CDR was usually measured manually by an ophthalmologist. This approach is ineffective and inefficient due to the tedious amount of work and the potentials for subjectivity. To address this problem, the recent approach includes an automated algorithm to measure CDR from retinal images obtained from a fundus camera. This allows effective and efficient measurement

doi: 10.18178/joig.10.3.109-115

of CDR and is even reliable for screening purpose due to fast detection.

There are two main approaches to automatically detect glaucoma from retinal images. The first approach implements an end-to-end deep learning model without explicit extraction of clinical features from retinal images as in [4], [5]. Nonetheless, this method is very sensitive to the quality difference of retinal image between training and the actual image. The second approach involves the extraction of clinical features such as CDR and neuroretinal rim, which requires segmentation of the Optic Disc (OD) and Optic Cup (OC) as in [2], [3], [6]-[8]. This method involves the localization of OD before segmentation to decrease computation complexity. The second method is preferable as it relies on segmentation performance and can be used for another task that requires OD and OC segmentation. Hence, our study is focused on the improvement of the OD localization and OD/OC segmentation algorithms. We optimize our algorithm specifically for Drishti-GS [9] and Refuge [10], [11] datasets which are available online.

The remainders of this paper are organized as follows. In Section II, we explain the previous method and its opportunity for improvement. In Section III, we elaborate on the proposed method. We report and discuss our result in Section IV and conclude it in Section V.

II. Related Works

There are several previous works on the localization and segmentation of OD/OC. The main objective of localization is to identify the most probable OD region such that the subsequent OD/OC segmentation algorithm can be confined in a much smaller region of interest. This process will markedly improve the segmentation efficiency since the OD region is usually sized less than 11% of the total retinal image [12]. Localization algorithms can be classified into two categories i.e., the supervised and unsupervised approaches. Supervised localization as in [6], [13], [14] utilize neural network architectures such as U-Net, Mask-RCNN, and Res-Net to localize OD. The unsupervised method used intensity-based thresholding and matching to localize OD. The thresholding localization method followed by grid selection is used in [12]. This method is prone to false-positive from other bright regions in the retina, such as exudates. Bright region detection followed by histogram template matching is used in [8]. However, the applied intensity threshold may exclude some of the OD regions. Furthermore, histogram template matching is also prone to false positives since it performs the localization without any spatial context.

For segmentation of OD/OC, unsupervised method is used in [2], [7], [8], [15]. Those methods are computationally inexpensive yet tend to have poor generalization capability since they were developed in very small datasets. Supervised methods provide better generalization as it involves learning from larger datasets. In [3], the superpixel classification method with SVM is used to segment OD/OC. Unfortunately, this method is computationally expensive and highly sensitive to variations in OD/OC dimension as well as in image contrast. In [6], [13], [14], [16] Fully Convolution Network (FCN) model such as U-Net, Res-Net, Mask-RCNN, DeepLabv3+ is used to perform pixel-wise semantic segmentation. These approaches produce a more detailed segmentation, thus increasing the segmentation performance significantly. However, they tend to be computationally expensive as well, especially with larger image dimensions, since the algorithm must consider the large variations within the total area of the retinal images. The computational cost can be reduced by confining the semantic segmentation algorithm to a certain Region of Interest (ROI), provided that the region of interest is sufficiently accurate in presenting candidates of OD regions. With a proper localization algorithm, we propose that an implementation of a basic semantic segmentation FCN model as U-Net may be sufficient to produce comparable performance concerning state-of-the-art semantic segmentation models.

III. Proposed Method

In general, our algorithm has two steps i.e., OD localization and OD/OC segmentation. Localization of OD is performed based on multiple maps created by weighted combinations of the Normalized Correlation Coefficient (NCC) map from OD template matching and image brightness. The predicted location of OD is defined by the location of the highest intensity in the combined map. A ROI sized 550×500 pixels is extracted from the original image with the location of OD as a center of ROI. The ROI is subsequently fed into the U-Net model [17] for segmentation of OD/OC. Lastly, segmentation of OD/OC is improved by implementing ellipse fitting.

A. OD Localization

The localization process receives RGB retinal image and produces an ROI image. We set the size of ROI to 550×550 pixels to accommodate the largest OD in Drishti-GS and Refuge that has a diameter of 514 pixels. The flowchart of localization is depicted in Fig. 2. First, NCC and brightness maps are extracted from the retinal image. From the experiment, we found that NCC maps from red and green channels give better localization which will be reported in Section IV. Thus, we use three maps i.e., red NCC, green NCC, and brightness map for the localization. Then, those three maps are weighted with $\alpha = 1$, $\beta = 0.8$, and $\gamma = 0.2$ respectively. The weights are obtained by grid search and manual tuning. Finally, the combined map is created by adding all those weighted maps. Predicted OD location is defined as the location of the highest intensity in the combined map. ROI with size 550×550 pixels is extracted from the green channel of the retinal image as the green channel has the highest local contrast than the other channels. To improve the sharpness of the ROI, we implement Contrast Limited Adaptive Histogram Equalization (CLAHE) with clip limit and tile grid parameter set to 2 and (8, 8) respectively.

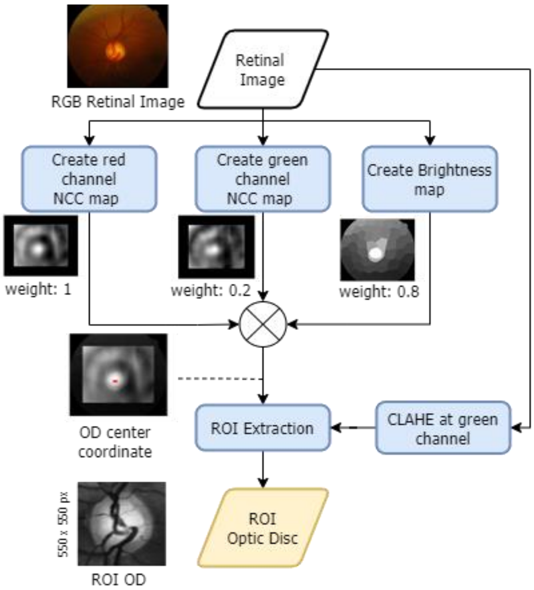

Figure 2. Multimap localization flowchart.

1) NCC map

NCC is calculated with (1) [18] based on a 550×550 pixels image template of OD derived from a subset of the training data. Unlike histogram template matching in [8], image-based correlation retains the spatial context of OD, leading to more robust performance. Fig. 3 shows the flowchart of the NCC calculation.

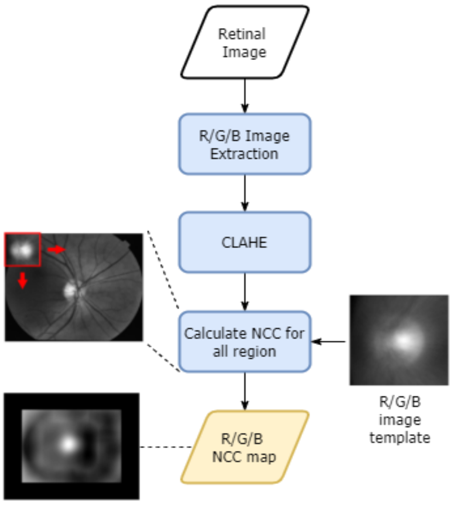

Figure 3. NCC map calculation flowchart.

$$NCC(x,y) = \frac{\sum_{x',y'}(T'(x',y')\cdot I'(x+x',y+y'))}{\sqrt{\sum_{x',y'}T'(x',y')^2\cdot\sum_{x',y'}I'(x+x',y+y')^2}} \quad (1)$$

where,

$$T'(x',y') = T(x',y') - \frac{\sum_{x'',y''}T(x'',y'')}{w\cdot h}$$

$$I'(x+x',y+y') = I(x+x',y+y') - \frac{\sum_{x'',y''}I(x+x'',y+y'')}{w\cdot h}$$

In (1), I is a greyscale image of one channel (R, G, or B) in the retinal image, T is the template image of the respective channel (R, G, or B), (x,y) is a coordinate in retinal images, (x',y') and (x'',y'') are a coordinate in the template image, w and h are width and height of template image. The template image was created by averaging 100 OD ROI that was extracted from the training image using the ground truth OD center for each channel. The images for creating the template are chosen such that the template could resemble OD appearance from Drishti-GS and Refuge. Before NCC calculation, CLAHE was implemented on the retinal image.

Previous works use a different approach to evaluate their localization methods. In [8], localization is considered successful when the center of ROI is included as the OD ground truth pixels which is a very loose criterion. On the other hand, in [12], the localization is considered successful when all of OD ground truth pixels are located within the ROI, which is a very strict criterion. We report our localization performance as the percentage of OD ground truth pixels that reside within the ROI.

2) Brightness map

A brightness map is utilized to improve OD localization by adding brightness information since OD is commonly the brightest region of the retinal image. Instead of using the threshold-based method [8], [12], we build a map that stores the highest intensity value in a certain region. Hence, the OD region could not inadvertently be removed. To segment the region in the retinal image, we generate 50 superpixels using Simple Linear Iterative Clustering (SLIC) [19].

The flowchart for creating a brightness map is depicted in Fig. 4. First, 50 superpixels are generated using the SLIC method. Before that, the image is resized with a scale of 0.125 and blurred with a 37×37 sized Gaussian kernel. The number of a superpixel, scaling factor, and kernel size parameters are tuned so that there is one superpixel can fit the OD region. After that, R, G, and B brightness maps are created by assigning the highest intensity of each segment for the R, G, and B channels. Then, those three brightness maps are averaged into one brightness map. Finally, the brightness map is rescaled to its original size.

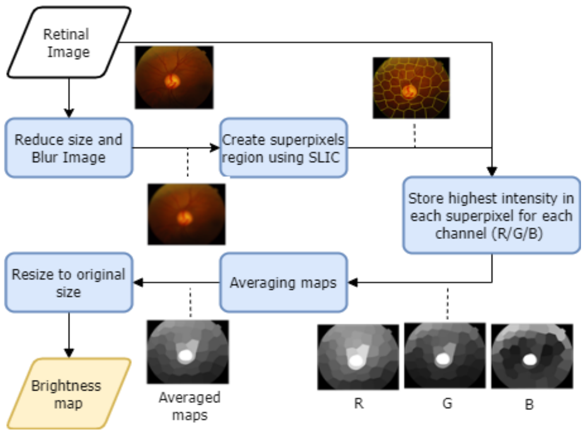

Figure 4. Brightness map creation flowchart.

B. Optic Disc and Optic Cup Segmentation

The segmentation process receives the ROI image from localization and creates OD/OC binary mask. After OD was localized, the ROI is downsampled to 256×256 pixels and then normalized. After that, OD and OC are segmented using different U-Net models, yet the input is the same. Then, OD and OC masks are upsampled to 550×550 pixels using bicubic interpolation. Finally, ellipse fitting is performed to OD and OC mask since OD and OC are typically in form of an ellipse. The flowchart of OD/OC segmentation is depicted in Fig. 5.

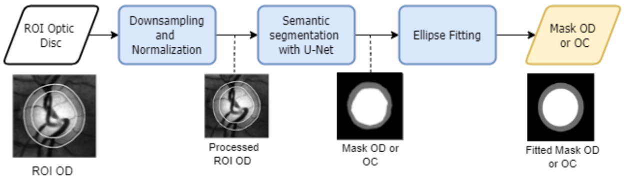

Figure 5. Segmentation of OD and OC flowchart.

U-Net is a Fully Convolution Network (FCN) founded by [17] that is specialized for segmentation of biological images. The architecture of U-Net can be seen in Fig. 6. We train the model with image data from Drishti-GS (50 images) and Refuge (400 images) with the ratio between train and test image set to 4:1. The hyperparameter for U-Net training is shown in Table I.

TABLE I. HYPERPARAMETER FOR THE TRAINING OF U-NET MODEL

Hyperparameter	Configuration	Description
Loss function	Binary cross-entropy	-
Batch size	16	-
Max epoch	100	Training is stopped when validation loss has not decreased for 20 epochs.
Dropout rate	0.1	Dropout layer is placed in every down sampling and up sampling block
Optimizer	Adam	-
Max learning rate	0.001	The learning rate is decreased by a factor of 0.1 when validation loss has not decreased for 5 epochs.

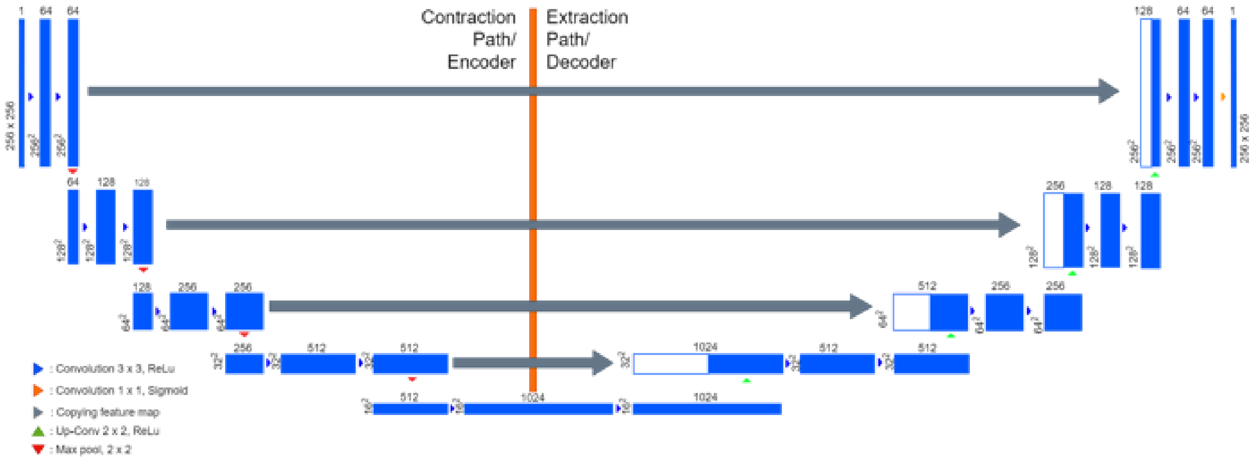

Figure 6. U-Net architecture for semantic segmentation of optic disc and optic cup.

We measured segmentation performance with F-score metrics as given in (2). F-score is ranged between 0-1. The segmentation whose F-score is close to 1 is a good segmentation and *vice versa*. True Positive (TP) is the amount of correctly classified pixel as part of the area, and True Negative (TN) is the amount of correctly classified pixel as part of non-area. On the other hand, False-Positive (FP) is the amount of falsely classified pixel as a part of the area, and negative (FN) is the amount of falsely classified pixel as a part of non-area.

$$F - score = \frac{2 \times TP}{2 \times TP + (FP + FN)} \tag{2}$$

IV. RESULT AND DISCUSSION

A. Dataset

We optimize our method on Drishti-GS [9] and Refuge [10], [11] dataset which are available online. The statistic of the dataset is shown in Table II. Although the resolution is similar, there exists a significant difference between Drishti-GS and Refuge. Drishti-GS's OD is located at the center of the image. Otherwise, Refuge's OD is located on the left side of the image. Furthermore, those datasets have different colors, textures, and contrast which can be seen in Fig. 7. Hence, to make a robust model, we set an equal proportion of samples from each dataset in train and test data with 4:1 as a ratio between train and test data.

TABLE II. THE STATISTIC OF THE DRISHTI-GS AND REFUGE DATASET USED IN THE EVALUATION

Dataset	Resolution	Number of samples
Drishti-GS	2047×1760	50 (41 train, 9 test)
Refuge	2124×2056	400 (320 train, 80 test)

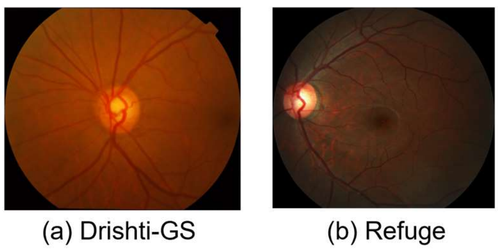

Figure 7. The difference between Drishti-GS and refuge image. There is a significant difference between these two datasets.

B. OD Localization

The best localization is achieved by combining weighted red NCC, green NCC, and brightness maps. As seen in the boxplot in Fig. 8, top-notch localization performance is achieved when red NCC, green NCC, and brightness maps are combined and weighted. This is because the NCC map is sensitive to ellipse-like objects besides OD such as cotton-wall spots and exudates. On the other hand, a brightness map is sensitive to bright regions whether it has an ellipse-like or irregular form. An irregular bright region such as bright fringe could alter localization when it has a higher intensity than OD. Luckily, the NCC map is not sensitive to the bright fringe. Therefore, combining those three maps could eliminate these problems.

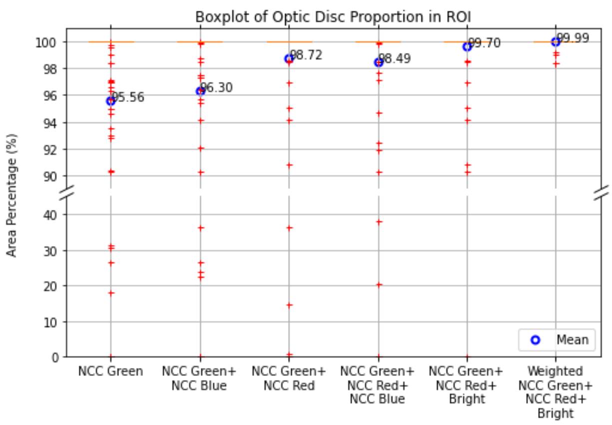

Figure 8. Boxplot of OD area in ROI. The best localization is achieved with NCC Red, NCC Green, and Brightness map with $\alpha = 1$, $\beta = 0.8$, and $\gamma = 0.2$ as weight respectively.

Unfortunately, we cannot compare our work with [8], [12] due to different datasets. Hence, we compare our work with the replication of the method used in [8], [12] on Drishti-GS and Refuge. Our method achieves 100% of the [8] metric and 99.1% of [12] metric with 99.99±0.12% of OD is captured in ROI. Localization performance is significantly increased compared to the replication method of [8], [12] as shown in Table III. This implies that the purposed method performs effectively on Drishti-GS and Refuge datasets.

From our findings, histogram template matching from [8] is less effective than image-based matching as it ignores the spatial context of OD. Thus, finding the robust OD histogram template for template matching is more challenging than the OD image template. Furthermore, thresholding-based bright detection from [8], [12] often excludes OD itself. Therefore, we use a brightness map that retains brightness information without inadvertently removing the OD region. However, there are four images that OD area is less than 100% as the image has a larger ONH than most of the images. Hence, the size of ROI should be optimized such that all OD is included in ROI.

TABLE III. Comparison with Previous Localization Methods on Drishti-GS and Refuge

Method	Mean area of OD in ROI (%)	Metric of [12] (%)	Metric of [8] (%)
Thresholding and grid selection [1] [12]	96.31 ± 14.15	66.7	78.9
Bright detection and Histogram Template Matching [2] [8]	98.74 ± 10.67	96.2	98.4
Proposed method	**99.99 ± 0.12**	**99.1**	**100**

C. OD and OC Segmentation

We evaluate our method with test images that have been localized with our segmentation method. We calculate the F-score of each test data and average it to get the mean F-score. The proposed method reached a competitive result compared to existing methods as shown in Table IV. On the Drishti-GS dataset, the proposed method achieved an F-score of 0.935±0.031 and 0.832±0.071 for OD and OC respectively. This result outperforms previous works in [8], [15], [20] for OD segmentation and [8], [20] for OC segmentation. However, our method yields a slightly lower F-score than [15], [16] for OC segmentation. On the Refuge dataset, the proposed method surpasses previous works in [13], [21] and competes with [14] for OD segmentation. For OC segmentation, our method surpassing previous methods from [13], [14], [21]. These results show that the proposed method is effective for the segmentation of OD and OC.

One of the main problems in OD/OC segmentation is blood vessels. Blood vessels on ONH could interfere the segmentation as it covers most of the ONH region. Methods that segment the OD and OC based on intensity such as k-means used in [8] often yield fragmented segmentation. To avoid this, in [2], blood vessel elimination is applied before segmentation. This leads to inefficiency since it required blood vessel segmentation which is a more complex process than OD and OC segmentation. On the other hand, semantic segmentation using a neural network such as U-Net could segment OD and OC without fragmenting the ONH region as the model learns how to transform the pixels in the input image as well as blood vessel pixels inside ONH into OD or OC region directly from its ground-truth marking.

The implementation of CLAHE and ellipse fitting on image increase the segmentation quality. CLAHE increases the contrast of OD and OC which makes the U-Net model easier to distinguish the feature of the regions. This leads to more robust segmentation. Although the shape of OD and OC is not purely ellipse, ellipse fitting could smooth the contour of OD and OC resulting from U-Net as well as correct the defective segmentation e.g., hollowed segmentation, or concave shape segmentation.

Due to an unbalanced dataset between Refuge and Drishti-GS, the U-Net model leans to yield better segmentation on Refuge images. The result should be increased if the model has been optimized for each dataset.

[1] The results are taken by replicating the [12] method on Drishti-GS and Refuge dataset.

[2] The results are taken by replicating the [8] method on Drishti-GS and Refuge dataset.

Unfortunately, the number of images from Drishti-GS is not enough to train a reliable U-Net model so the model is still trained with an amalgamation of Refuge and Drishti-GS. For further research, we suggest using data augmentation to improve segmentation performance in each dataset.

TABLE IV. SEGMENTATION RESULT OF THE PROPOSED METHOD IN DRISHTI-GS AND REFUGE DATASET

Dataset	Method	Mean F-score OD	Mean F-score OC
Drishti-GS	Level-set based [20]	0.911	0.771
	Active Disc [15]	0.928	0.753
	Semantic Segmentation U-net [16]	-	**0.850**
	Kmeans and Hough Circle Fitting [8]	0.915	0.790
	Proposed method	**0.935 ± 0.031**	0.832 ± 0.071
Refuge	DeepLab v3+ with pixel quantification [21]	0.949	0.864
	FCNs ResNet-50, -101, -152, -38 [14]	**0.951**	0.867
	Mask-RCNN and U-shaped dense network [13]	0.936	0.867
	Proposed method	0.950 ± 0.028	**0.871 ± 0.061**

V. CONCLUSION

The proposed method yields competitive results with state-of-the-art works. Our localization method successfully detects all locations of OD with 99.99±0.12% of OD is captured in ROI. Optimizing the size of ROI would improve the localization so cropped OD will be minimized. Then, our segmentation method achieves top-notch results. On the Drishti-GS dataset, the proposed method achieves 0.935±0.031 of F-score OD and 0.832±0.071 of F-score OC. On the Refuge dataset, the proposed method achieves 0.950±0.028 of F-score OD and 0.871±0.061 of F-score OC. This implies that the proposed method could effectively implemented on Drishti-GS and Refuge.

For further research, we suggest applying image augmentation to improve the segmentation performance. We also suggest continuing the research of superpixel as it has the potential to be the only localization map instead of adding an NCC map so the localization will be much simpler and robust, and even could directly segment OD or OC in an unsupervised way.

CONFLICT OF INTEREST

The authors declare no conflict of interest.

AUTHOR CONTRIBUTIONS

A. N. Almustofa conducted the research, analyzed data, created the solution, and wrote the paper; A. Handayani supervised the research, created the solution, and wrote the paper; T. L. R. Mengko supervised the research; all authors had approved the final version.

REFERENCES

[1] Infodatin. (2019). Glaucoma situation in Indonesia. Ministry of Health Republic of Indonesia. [Online]. pp. 1-12. Available: https://www.pusdatin.kemkes.go.id/resources/download/pusdatin/infodatin/infoDatin_glaukoma_2019.pdf

[2] P. S. Mittapalli and G. B. Kande, "Segmentation of optic disk and optic cup from digital fundus images for the assessment of glaucoma," *Biomedical Signal Processing and Control*, vol. 24, pp. 34-46, 2016.

[3] J. Cheng, *et al.*, "Superpixel classification based optic disc and optic cup segmentation for glaucoma screening," *IEEE Transactions on Medical Imaging*, vol. 32, no. 6, pp. 1019-1032, 2013.

[4] A. Diaz-Pinto, S. Morales, V. Naranjo, T. Köhler, J. M. Mossi, and A. Navea, "CNNs for automatic glaucoma assessment using fundus images: An extensive validation," *BioMedical Engineering OnLine*, vol. 18, no. 1, p. 29, 2019.

[5] A. Saxena, A. Vyas, L. Parashar, and U. Singh, "A glaucoma detection using convolutional neural network," in *Proc. International Conference on Electronics and Sustainable Communication Systems*, 2020, pp. 815-820.

[6] S. Wang, L. Yu, X. Yang, C. W. Fu, and P. A. Heng, "Patch-Based output space adversarial learning for joint optic disc and cup segmentation," *arXiv*, vol. 38, no. 11, pp. 2485-2495, 2019.

[7] H. Ahmad, A. Yamin, A. Shakeel, S. O. Gillani, and U. Ansari, "Detection of glaucoma using retinal fundus images," in *Proc. International Conference on Robotics and Emerging Allied Technologies in Engineering*, 2014, pp. 321-324.

[8] A. Mvoulana, R. Kachouri, and M. Akil, "Fully automated method for glaucoma screening using robust optic nerve head detection and unsupervised segmentation based cup-to-disc ratio computation in retinal fundus images," *Computerized Medical Imaging and Graphics*, vol. 77, p. 101643, 2019.

[9] J. Sivaswamy, S. R. Krishnadas, G. D. Joshi, M. J. Ujjwal, and S. Tabish, "Drishti-GS: Retinal image dataset for Optic Nerve Head (ONH) segmentation," in *Proc. IEEE 11th International Symposium on Biomedical Imaging*, 2014, pp. 53-56.

[10] J. I. Orlando, *et al.*, "REFUGE challenge: A unified framework for evaluating automated methods for glaucoma assessment from fundus photographs," *Medical Image Analysis*, vol. 59, 2020.

[11] F. Li, *et al.*, "Development and clinical deployment of a smartphone-based visual field deep learning system for glaucoma detection," *npj Digital Medicine*, vol. 3, no. 1, 2020.

[12] Z. Zhang, *et al.*, "Optic disc region of interest localization in fundus image for glaucoma detection in ARGALI," in *Proc. 5th IEEE Conference on Industrial Electronics and Applications*, 2020, pp. 1686-1689.

[13] X. Bian, Y. Huang, X. Li, X. Niu, J. Wu, and Y. Xie, "Automatic optic disc / cup segmentation and glaucoma classification and fovea localization," *Refuge Reports*, pp. 1-13, 2020.

[14] Z. Wu, C. Shen, A. V. D. Hengel, and J. Zhang. Optic disc / cup segmentation and glaucoma classification from fundus images with fully convolutional networks. [Online]. pp. 2-4. Available: http://rumc-gcorg-p-public.s3.amazonaws.com/f/challenge/229/3e7a9944-5121-4bc8-848b-ac6115d39748/REFUGE-AIML.pdf

[15] J. R. H. Kumar, C. S. Seelamantula, Y. S. Kamath, and R. Jampala, "Rim-to-Disc ratio outperforms cup-to-disc ratio for glaucoma prescreening," *Scientific Reports*, vol. 9, no. 1, pp. 1-9, 2019.

[16] A. Sevastopolsky, "Optic disc and cup segmentation methods for glaucoma detection with modification of U-net convolutional neural network," *Pattern Recognition and Image Analysis*, vol. 27, no. 3, pp. 618-624, 2017.

[17] O. Ronneberger, P. Fischer, and T. Brox, "U-Net: Convolutional networks for biomedical image segmentation," in *Proc. Medical Image Computing and Computer-Assisted Intervention*, 2015, pp. 234-241.

[18] A. Kaehler and G. Bradski, *Learning OpenCV 3: Computer Vision in C++ with the OpenCV Library*, O'Reilly Media, 2016.

[19] R. Achanta, A. Shaji, K. Smith, A. Lucchi, P. Fua, and S. Süsstrunk, "SLIC superpixels compared to state-of-the-art superpixel

methods," *IEEE Transactions on Pattern Analysis and Machine Intelligence*, vol. 34, no. 11, pp. 2274-2282, 2012.

[20] D. K. Wong, *et al.*, "Level-set based automatic cup-to-disc ratio determination using retinal fundus images in ARGALI," in *Proc. Annual International Conference of the IEEE Engineering in Medicine and Biology Society*, vol. 2008, pp. 2266-2269, 2008.

[21] H. Kang, K. Wang, S. Guo, Y. Gao, N. Li, and J. Weng. Pixel quantification for robust segmentation of optic cup. [Online]. Available: http://rumc-gcorg-p-public.s3.amazonaws.com/f/challenge/229/64244eec-3800-4dda-a882-229eb924d277/REFUGE-NKSG.pdf

A. N. Almustofa (born in Bekasi, Indonesia) earned his Bachelor Degrees in biomedical engineering from Department of Biomedical Engineering, Bandung Institute of Technology (Bandung, Indonesia) in 2021. In 2020, he had internship in government task force for handling Covid-19 pandemic in technological aspects as a Performance Analyst. In 2021, He had been trained as machine learning specialist for six months at Bangkit Academy 2021 held by Google Indonesia, and various unicorn company in Indonesia.

A. Handayani (born in Bandung, Indonesia) earned her Bachelor and Master Degrees in electrical engineering (Biomedical Engineering) from the Department of Electrical Engineering, Bandung Institute of Technology, in 2004 and 2006, respectively. Since 2015, she joined the School of Electrical Engineering and Informatics, Bandung Institute of Technology as a lecturer at the Biomedical Engineering Bachelor Study Program and a member of Biomedical Research Division. Her current research interests include: medical image processing and medical imaging. She is a member of the Indonesian Biomedical Engineering Society and IEEE-EMBS.

T. L. R. Mengko (born in Surabaya, Indonesia) earned her Bachelor Degrees in electrical engineering (Electronics) from the Department of Electrical Engineering, Bandung Institute of Technology in 1977. She obtained the doctorate degree from ENSERG-INP Grenoble France (Image Processing) in 1985. She joined the Department of Electrical Engineering ITB since 1977, Head of Department from 1995-1998, Head of Microelectronics Inter University Research Centre in 1999, and Dean of Faculty of Industrial Technology in 2001. She then became a professor at the School of Electrical Engineering and Informatics in 2006. She is currently Head of Biomedical Research Division in School of Electrical Engineering and Informatics. Her current research interests include: image processing, medical imaging and instrumentation, e-health. She is a member of the Indonesian Biomedical Engineering Society and IEEE-EMBS.